Behavioral/Systems/Cognitive

Effective Deep Brain Stimulation Suppresses Low-Frequency Network Oscillations in the Basal Ganglia by Regularizing Neural Firing Patterns

George C. McConnell,[1]* Rosa Q. So,[1]* Justin D. Hilliard,[1] Paola Lopomo,[1] and Warren M. Grill[1,2,3]
Departments of [1]Biomedical Engineering, [2]Neurobiology, and [3]Surgery, Duke University, Durham, North Carolina 27708

Deep brain stimulation (DBS) of the subthalamic nucleus (STN) is an effective treatment for the motor symptoms of Parkinson's disease (PD). The effects of DBS depend strongly on stimulation frequency: high frequencies (>90 Hz) improve motor symptoms, while low frequencies (<50 Hz) are either ineffective or exacerbate symptoms. The neuronal basis for these frequency-dependent effects of DBS is unclear. The effects of different frequencies of STN-DBS on behavior and single-unit neuronal activity in the basal ganglia were studied in the unilateral 6-hydroxydopamine lesioned rat model of PD. Only high-frequency DBS reversed motor symptoms, and the effectiveness of DBS depended strongly on stimulation frequency in a manner reminiscent of its clinical effects in persons with PD. Quantification of single-unit activity in the globus pallidus externa (GPe) and substantia nigra reticulata (SNr) revealed that high-frequency DBS, but not low-frequency DBS, reduced pathological low-frequency oscillations (~9 Hz) and entrained neurons to fire at the stimulation frequency. Similarly, the coherence between simultaneously recorded pairs of neurons within and across GPe and SNr shifted from the pathological low-frequency band to the stimulation frequency during high-frequency DBS, but not during low-frequency DBS. The changes in firing patterns in basal ganglia neurons were not correlated with changes in firing rate. These results indicate that high-frequency DBS is more effective than low-frequency DBS, not as a result of changes in firing rate, but rather due to its ability to replace pathological low-frequency network oscillations with a regularized pattern of neuronal firing.

Introduction

Deep brain stimulation (DBS) improves motor symptoms in persons with Parkinson's disease (PD) (Deuschl et al., 2006), but the mechanisms of action remain unclear (McIntyre and Hahn, 2010). Alleviation of symptoms including tremor, bradykinesia, and rigidity depends strongly on the frequency of stimulation: high-frequency stimulation (HFS) (>90 Hz) is required for efficacy, while low-frequency stimulation (LFS) (<50 Hz) is ineffective or worsens motor symptoms (Birdno and Grill, 2008). The goal of this study was to use the frequency-dependent effects of DBS on motor symptoms as a basis to investigate underlying neuronal mechanisms.

One proposed mechanism of DBS is a change in basal ganglia neuronal firing patterns during stimulation. Both computational studies (Terman et al., 2002; Grill et al., 2004; Rubin and Terman, 2004; So et al., 2012b) and experimental studies (Hashimoto et al., 2003; Dorval et al., 2008; Rosin et al., 2011) have shown that HFS is effective at overriding intrinsic pathological neuronal activity and regularizing neuronal firing patterns. However, some neuronal recordings were conducted in brain slices or anesthetized animals, and the corresponding behavioral efficacy was not established. As well, the majority of behavioral studies were conducted at only one stimulation frequency (130 Hz). In contrast, we studied systematically and quantitatively the relationship between symptoms and changes in neuronal activity across a wide range of DBS frequencies.

Using a rat model of PD, we correlated the changes in motor symptoms with changes in neuronal activity across a broad range of frequencies of DBS. Results from two types of behavioral tests showed that the effects of stimulation frequency in the rat paralleled clinical observations in humans, with high frequencies required for efficacy. This frequency dependence formed the basis for studying the changes in neuronal activity during DBS. We quantified features of neuronal firing within the globus pallidus externa (GPe) and substantia nigra reticulata (SNr) that were associated with therapeutically effective DBS. There was no significant change in the mean firing rates of GPe and SNr neurons during DBS, but there were significant stimulation frequency-dependent changes in firing patterns. HFS, but not LFS, reduced low-frequency neuronal oscillations, increased neuronal oscillations at the stimulation frequency, and increased phase locking with the stimulus pulses. Moreover, coherence within and across the GPe and SNr during HFS was reduced in the

Received June 13, 2012; revised Aug. 11, 2012; accepted Aug. 31, 2012.

Author contributions: G.C.M., R.Q.S., and W.M.G. designed research; G.C.M., R.Q.S., J.D.H., and P.L. performed research; G.C.M. and R.Q.S. analyzed data; G.C.M., R.Q.S., and W.M.G. wrote the paper.

This research was supported by NIH Grants R01 NS040894 (W.M.G.) and T32 NS051156 (G.C.M.), the A*STAR NSS-PhD scholarship program (R.Q.S.), and the Howard Hughes Medical Institute Medical Fellows Program (J.D.H.). We thank M.-Y. Chen for assistance with histology and data analysis; A. August for assistance with histology; and G. Mills for laboratory support.

*G.C.M. and R.Q.S. contributed equally to this work.

Correspondence should be addressed to Warren M. Grill, Duke University, Department of Biomedical Engineering, Box 90281, Durham, NC 27708-0281. E-mail: warren.grill@duke.edu.

DOI:10.1523/JNEUROSCI.2824-12.2012

 0270-6474/12/3215657-12$15.00/0

band of pathological low-frequency oscillations and increased in the stimulation frequency band.

These findings provide evidence that effective high-frequency DBS suppresses low-frequency network oscillations and entrains neurons in the basal ganglia. Therefore, the present results support the hypothesis that the effectiveness of HFS stems from its ability to override pathological firing patterns in the basal ganglia by inducing a new regularized pattern of synchronous neuronal activity.

Materials and Methods

Surgical procedures

Chronic electrode implants. All animal care and experimental procedures were approved by the Duke University Institutional Animal Care and Use Committee. Long–Evans female rats (250–350 g) were anesthetized using a mixture of 5% isoflurane and 1 L min^{-1} O_2 and positioned into a stereotaxic frame (Kopf) where anesthesia was maintained to effect (~1–3% isoflurane and 0.3 L min^{-1} O_2) during surgery. Rats were implanted unilaterally with a cannula placed in the medial forebrain bundle (MFB) (anteroposterior (AP), 2.0 mm and mediolateral (ML), 2.0 mm from bregma; dorsoventral (DV), 7.5 mm from the surface of the brain) and a four-channel platinum-iridium stimulating microelectrode array (MEA; Microprobes) placed in the subthalamic nucleus (STN) (AP, 3.6 mm and ML, 2.6 mm from bregma; DV, 6.6–6.9 mm from the surface of the brain). The stimulating electrodes were 75 μm in diameter arranged in a 2 × 2 array with 600 μm spacing and had an impedance of 10 kΩ at 1 kHz. The 16-channel recording electrodes were implanted unilaterally in the GPe (AP, 0.5–1.5 mm and ML, 2.5–3.5 mm from bregma; DV, 4.5–5.0 mm from the surface of the brain) and the SNr (AP, 5.7 mm and ML, 1.2–2.7 mm from bregma; DV, 7.5–8.0 mm from the surface of the brain). All stereotaxic coordinates referenced above are according to the stereotaxic atlas of Paxinos and Watson (2007). Eight stainless steel screws were anchored to the skull, with one screw placed over the cerebellum used as a reference electrode for neuronal recordings. The implanted microelectrode arrays and cannula were secured to the screws using dental acrylic.

6-OHDA lesioning. After 1 week of recovery, 6-hydroxydopamine (6-OHDA) was infused into the MFB of one hemisphere to induce unilateral degeneration of the dopaminergic neurons in the substantia nigra pars compacta (SNc). Rats were anesthetized using a mixture of 5% isoflurane and 1 L min^{-1} O_2 and were positioned into a stereotaxic frame where anesthesia was maintained to effect (~1–3% isoflurane and 0.3 L min^{-1} O_2) during surgery. Rats were pretreated with 50 mg/kg, i.p., pargyline (Sigma-Aldrich) to inhibit monoamine oxidase and 5 mg/kg, i.p., desipramine (Sigma-Aldrich) to protect noradrenergic neurons 30 min before infusing 6-OHDA (Breese and Traylor, 1971). Immediately before infusion, 6-OHDA (Sigma-Aldrich) was dissolved in ice-cold 0.2% ascorbic acid dissolved in normal saline. Ten microliters of 10 mM 6-OHDA was infused through the cannula at a rate of 2 μl/min. The rats were then allowed to recover for 1 week before commencing stimulation and behavioral experiments. In cases when a rat did not exhibit motor deficits following lesioning, we performed up to two additional 6-OHDA injections.

Behavioral tests

Methamphetamine-induced circling. Methamphetamine-induced circling was quantified in unilateral 6-OHDA-lesioned rats, as previously described (So et al., 2012a). During each experiment, the rat was administered a single dose of methamphetamine (Sigma-Aldrich) (1.25–2.5 mg/kg in normal saline, i.p.) and then placed in a dark 30 cm diameter cylindrical chamber equipped with an infrared camera that captured the rat's activity for 2 h. During this time, four blocks of 10 different frequencies of DBS were delivered for a total of 40 stimulation periods, with presentation order randomized within each block. Stimulation epochs of 1 min duration were delivered 3 min apart, allowing 2 min of rest between each pattern to minimize carry over effects, and repeated experiments were performed at least 2 d apart.

Behavioral analysis software (CleverSys) was used to quantify the position of the nose and the base of tail over time. Angular velocity and distance traveled were calculated from the tracking data using MATLAB (version 7.4; Mathworks). Normalized angular velocity for each trial was calculated by dividing the angular velocity during the 1 min "DBS-on" period by the average angular velocities during the 1 min "pre-DBS-off" and "post-DBS-off" periods immediately before and after the DBS-on period. Normalized angular velocities and normalized distances traveled for each stimulation frequency were then calculated by averaging across the four randomized blocks. Normalization reduced variability in circling rates across different rats and within each rat during an experimental session due to the time course of the drug effect (So et al., 2012a).

Haloperidol-induced akinesia. Systemic administration of haloperidol, a dopamine receptor antagonist, was used as a model of akinesia and rigidity in PD (Sanberg et al., 1988). Haloperidol experiments were performed on 6-OHDA-lesioned rats after the completion of methamphetamine-induced circling experiments. Due to differences in DA receptor expression caused by lesioning, the dose of haloperidol for each rat (range: 0.5–5 mg/kg) was titrated to the minimum dose that resulted in ataxia (defined as the rat staying on the bar for >5 min). The dose was determined empirically starting at a low dose and increasing in a subsequent experiment if the rat was not ataxic. This dose was then maintained for the remaining experiments testing different stimulation frequencies. The degree of akinesia was assessed using a bar grip test. The rat was injected with haloperidol (0.5–5 mg/kg, i.p.). After a period of 10 min, the forelimbs were placed on a bar raised 10 cm from the ground, and the time to touch one forelimb to the ground was recorded (i.e., the time for it to release its grip). A maximum grip time of 5 min was allowed, after which the rat was removed from the bar. Testing was repeated every 10 min for 60 min. Continuous stimulation for each stimulation condition (a total of five different stimulation frequencies in addition to a no-stimulation control) began 35 min postinjection. The order of stimulation conditions presented was randomized for each rat to control for order effects. Haloperidol experiments were performed with at least 1 d in between to minimize carryover effects.

Stimulation parameters

Stimulation was delivered to the STN through the stimulating MEA via an isolated voltage-to-current converter (A-M Systems) controlled by MATLAB. Charge-balanced biphasic pulses with a pulse width of 90 μs were delivered with amplitudes ranging from 50 to 200 μA. The amplitude of stimulation for each rat was determined based on tuning (immediately following methamphetamine injection in the case of the circling test, before haloperidol injection in the case of the bar test, or before starting neuronal recordings). The stimulation amplitude was selected based on effectiveness in eliciting sustained motor responses to 130 Hz stimulation, which included decreased ipsilateral turning, increased contralateral turning, increased activity, increased rearing, as well as a lack of motor side effects such as involuntary muscle contractions of the limbs and neck (circling: 68 ± 30 μA, n = 13; bar test: 61 ± 35 μA, n = 10; neural recordings: 42 ± 22 μA, n = 11; values are mean ± SD). All experiments were conducted using a range of stimulation frequencies between 5 and 260 Hz, with fixed stimulation amplitude.

Single-unit neuronal recording

Single-unit neuronal activity was recorded using a multichannel acquisition processor system (Plexon). Thirty-two channels were recorded simultaneously while the rats were awake and resting inside a Faraday cage (gain = 50; filter = 150 Hz–8.8 kHz; sampling rate = 40 kHz). Recordings were made during two different sessions: just before 6-OHDA lesioning and at least 1 week after 6-OHDA lesioning with and without DBS. The prelesion recording session was a total of 20 min in duration. The recording session made after 6-OHDA lesioning was a total of 1 h and 15 min in duration (5 stimulation conditions × 15 min each condition). For each condition, there was a 5 min DBS-off period (pre-stim), followed by a 5 min DBS-on period (stim), followed by a 5 min DBS-off period (post-stim).

Single-unit neuronal recording analysis

Neuronal recordings were sorted on-line and further refined off-line using Offline Sorter (Plexon). Isolated units were verified based on the presence of a refractory period in the interspike interval (ISI) histogram, and further analysis was limited to well isolated units. The spike times of sorted units were further processed in MATLAB.

For each rat, a template of the stimulation artifact was created using Offline Sorter to quantify the times that artifacts occurred and to gener-

ate post-stimulus time histograms (PSTHs) for all units. To control for stimulation artifacts, a blanking mask was created by adding the blanking period (range: 0.5–2 ms) to each stimulation artifact timestamp and applied to both the pre-stim and post-stim periods. The blanking period was based on the duration of the stimulation artifact as indicated by the period devoid of activity across all units in the PSTH (Fig. 1*D*).

Firing rates across time were analyzed by binning the spike times into 5 s bins (Fig. 1*A*). Neurons were categorized by their change in firing rate during DBS into the following three groups: (1) decreased firing rate, (2) increased firing rate, or (3) no change in firing rate using a Student's *t* test. ISI histograms were generated for pre-stim, stim, and post-stim conditions (bin size = 1 ms; Fig. 1*B*). Spectral analysis of the spike times was used to quantify temporal structure in the data (Chronux version 2.00; Fig. 1*C*). Multitaper methods of spectral estimation were used to construct spectral estimators (Mitra and Pesaran, 1999). The spike spectrum was estimated on a 5 s window with 10 Hz resolution using 5 Slepian data tapers. Spectral power in bands of interest was quantified by first correcting for differences in baseline power. A line of best fit constructed from points outside the band of interest was subtracted from the power within the band of interest, and the baseline-corrected spectral power was then integrated over the band of interest. Coherence spectra of unique sets of simultaneously recorded neuronal pairs were constructed using a 10 s window using 5 Slepian data tapers (Fig. 1*E*). Neuron pairs were categorized by their change in coherence during DBS into the following three groups: (1) decreased coherence, (2) increased coherence, or (3) no change in coherence using a Student's *t* test.

Vector strength (VS) was used to quantify the synchronization of neuronal responses to different stimulation frequencies (Goldberg and Brown, 1969). The latency of each spike from the preceding stimulus pulse was expressed as an angle (θ) between 0 and 2π radians mapped across the interstimulus period. The vectors were geometrically averaged to obtain the magnitude, which was then normalized by the number of spikes analyzed (n).

$$\mathrm{VS} = \frac{\sqrt{\sum(\sin(\theta))^2 + \sum(\cos(\theta))^2}}{n}.$$

Histology

Histology was used to assess the extent of the 6-OHDA lesion (Fig. 2*A*) and the locations of stimulation electrodes (Fig. 2*B*) and recording electrodes (Fig. 2*C*, SNr; Fig. 2*D*, GPe). Each animal was deeply anesthetized with pentobarbital (100 mg kg^{-1}, i.p.) and transcardially perfused with PBS followed by 10% formalin. The brain was removed and postfixed overnight (4°C) in formalin then placed in a 30% sucrose (4°C) solution until it sank. A tissue dye was applied to the left-posterior hemisphere to identify later the orientation of the brain sections. The brains were cryoprotected with an optimal cutting temperature compound (Tissue-Tek O.C.T.), and 50 μm serial sections were cut using a cryostat. After five rinses in PBS, sections were incubated for 10 min in 3% hydrogen peroxide. The sections were rinsed, and blocked for 1 h at 4°C in blocking solution containing 8% horse serum, avidin (10 $\mu g\ ml^{-1}$), and 0.1% Triton-X. The sections were then incubated in anti-tyrosine hydroxylase (anti-TH; monoclonal mouse IgG1; 1:1000 overnight at 4°C; Sigma-Aldrich) in solution with 2% horse serum and biotin (50 $\mu g\ ml^{-1}$). Next, the sections were incubated with biotinylated horse anti-mouse secondary antibody (1:200 for 1 h at 4°C; Vector Laboratories), and then visualized using a VECTASTAIN Elite ABC kit (Vector Laboratories). Sections were counterstained with cresyl violet.

TH-labeled SNc cells on both the lesioned and nonlesioned sides were counted under a light microscope. The percentage of dopaminergic cell loss was calculated as follows:

$$\%\ \text{dopaminergic cell loss} = \left(1 - \frac{\text{No. of TH labeled cells on lesioned side}}{\text{No. of TH labeled cells on nonlesioned side}}\right) \times 100$$

Cytochrome oxidase (CO), a mitochondrial enzyme correlated with neuronal activity, was stained to identify the STN. Tissue sections were suspended in CO staining solution (10 mg DAB (Sigma-Aldrich), 5 mg of cytochrome C (Sigma-Aldrich), and 0.8 g of sucrose dissolved in 0.1 M phosphate buffer for at least 6 h.

Only behavioral and neuronal data from rats with >90% dopaminergic cell loss in the lesioned hemisphere and with at least one stimulation electrode located in the STN were analyzed. Only units recorded from electrodes determined to be within the GPe and SNr were included for analysis.

Statistical analysis

Statistical inferences were made between differing conditions using either one-way or two-way ANOVA with repeated measures. When we found a significant factor, we performed the Fisher's protected least significant difference (PLSD) *post hoc* test to identify pairwise differences. Student's *t* test and Pearson's χ^2 test were used where indicated. All results are presented as the mean ± SE and were considered significant at $p < 0.05$.

Results

Histological analysis of 6-OHDA lesion and electrode locations

All 13 rats had >90% loss of TH-positive neurons in the lesioned hemisphere (Fig. 2*A*). In addition, all rats had at least one of the pair of STN electrodes used for bipolar stimulation placed within the STN (Fig. 2*B*,*E*). Of 11 rats from which we obtained neuronal recordings, recording electrodes were placed within the GPe in 7 rats (Fig. 2*D*) and the SNr in 7 rats (Fig. 2*C*), and 3 rats had electrodes in both GPe and SNr. Only units recorded from electrodes determined to lie in the target regions were analyzed.

Behavioral effects of STN-DBS frequency: circling

Ten different frequencies of DBS from 5 to 260 Hz were delivered to the STN in 13 6-OHDA unilaterally lesioned rats. The rats were injected with methamphetamine, which resulted in pathological turning ipsilateral to the lesion (Schwarting and Huston, 1996). Effective DBS resulted in a reversal of pathological turning behavior reflected as a decrease in normalized angular velocity compared with the off condition.

Frequency tuning curves for circling showed decreased ipsilateral turning (i.e., efficacy) with increased stimulation frequency (Fig. 3*A*). The normalized angular velocity of zero or less indicated that the rats showed either equal turning in both directions or increased turning in the contralateral direction. Since a decrease in angular velocity could simply be due to a lack of general movement, the distance the rat traveled in the cylinder was also quantified. Consistent with clinically effective DBS, HFS did not decrease movement of the rats, but rather facilitated it compared with LFS (Fig. 3*B*). Together, these results show that HFS reversed the pathological directional bias of unilaterally 6-OHDA-lesioned rats without inhibiting movement.

Behavioral effects of STN-DBS frequency: akinesia

We quantified the effects of DBS frequency on akinesia following administration of haloperidol in a subset of 10 rats from which circling data were previously collected. High-frequency DBS (130 and 185 Hz) significantly decreased the grip time on the bar compared with 75, 30, and 10 Hz, and no stimulation (Fig. 4). The effectiveness of HFS at reducing time spent on the bar was sustained through the 30 min period of stimulation (Fig. 4).

Neuronal effects of STN-DBS frequency: firing rate and pattern

Single units were recorded from the GPe (prelesion: 91 neurons; postlesion: 62 neurons) in seven rats and the SNr (prelesion: 70 neurons; postlesion: 51 neurons) in seven rats.

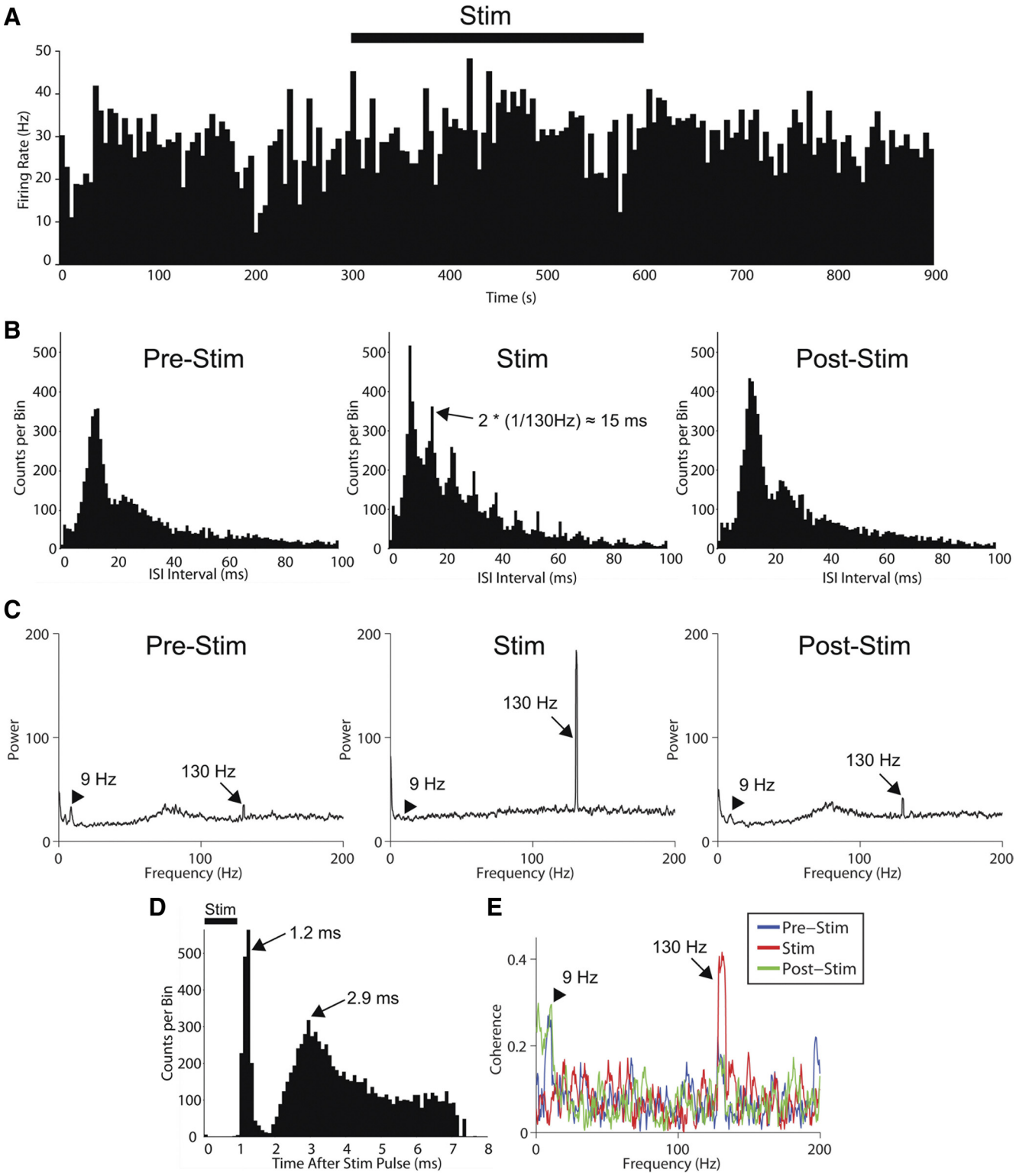

Figure 1. Example of analysis of the effects of DBS on the activity of one single unit recorded in GPe. ***A***, Firing rate over a 15 min recording session. Bar indicates 130 Hz STN-DBS. Firing rate of this unit did not change during DBS. Bin size = 5 s. ***B***, ISI histograms before (pre-stim), during (stim), and after (post-stim) stimulation. Peaks during stimulation indicate that the neuron fired at integer multiples of the interpulse interval (IPI). Arrow indicates second harmonic of the IPI. Bin size = 1 ms. ***C***, Spectral power pre-stim, stim, and post-stim. Low-frequency peak at ~9 Hz present in pre-stim and post-stim periods was reduced during DBS (arrowheads). Power at stimulation frequency of 130 Hz was increased during DBS (arrows). Peaks at 130 Hz during the pre-stim and post-stim periods are due to blanking periods inserted at the stimulation frequency (arrows). ***D***, PSTH. Peaks at 1.2 and 2.9 ms (arrows) indicate that this neuron fired at regular intervals during DBS. Bar indicates stimulation artifact. Bin size = 0.1 ms. ***E***, Coherence between single unit analyzed in ***A–D*** and another single unit recorded simultaneously in SNr over the pre-stim, stim, and post-stim periods. Coherence significantly decreased from pre-stim to stim and post-stim to stim only at 7–10 Hz ($p < 0.05$). Coherence significantly increased from pre-stim to stim and post-stim to stim only at 128–133 Hz ($p < 0.05$). There were no significant differences in coherence between pre-stim and post-stim conditions. Significance levels were calculated from estimates of the variance using a jackknife over tapers and 10 s segments (Bokil et al., 2007).

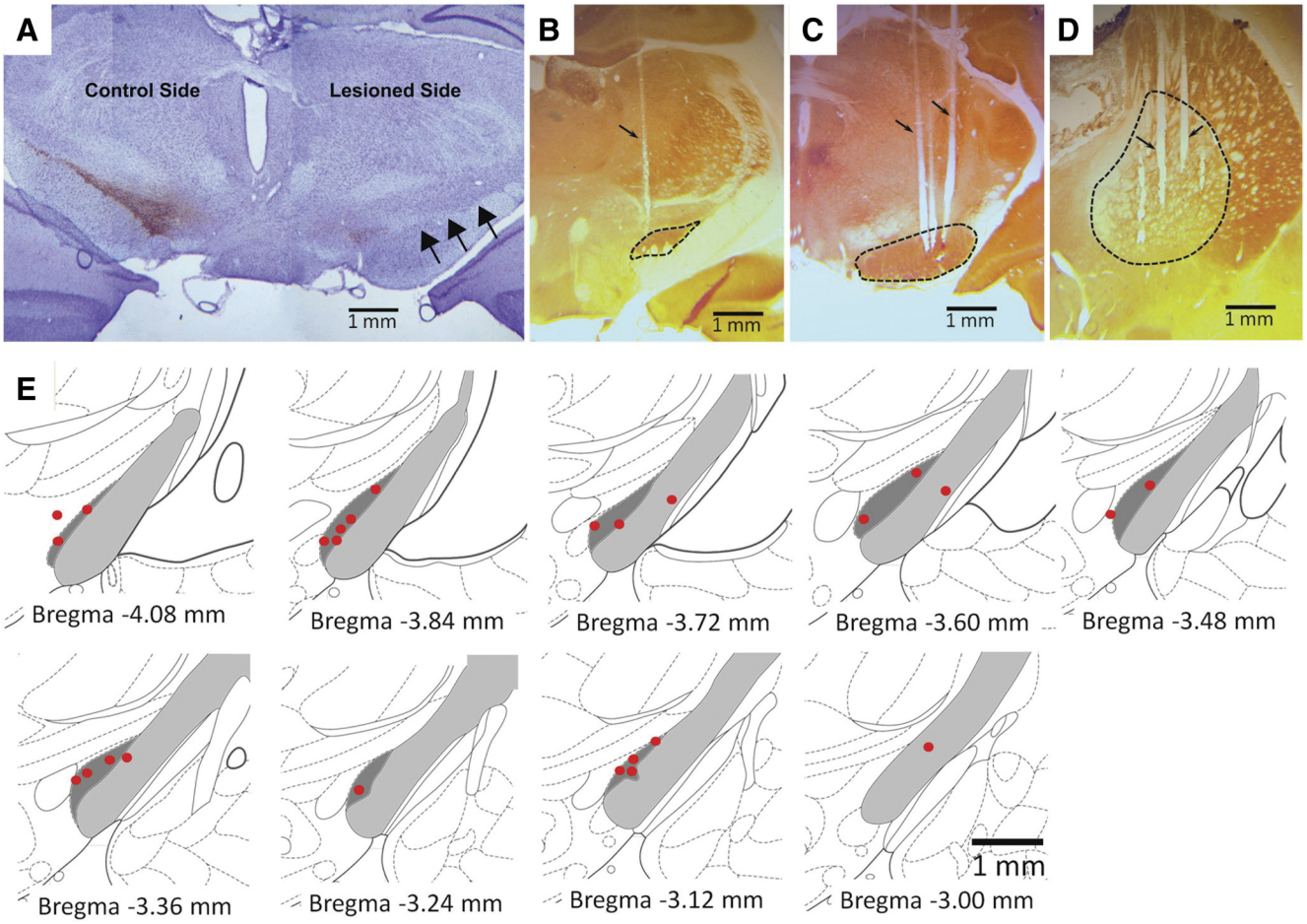

Figure 2. Histological evaluation of extent of dopaminergic cell loss and location of stimulating and recording electrodes. ***A***, Coronal section from a 6-OHDA-lesioned rat immunostained for tyrosine hydroxylase (brown) and counterstained with cresyl violet (purple). Note dopaminergic cell loss in SNc on lesioned side (arrows). ***B–D***, Coronal sections from a 6-OHDA-lesioned rat stained for cytochrome oxidase. Dashed lines indicate borders of STN (***B***), SNr (***C***), and GPe (***D***). ***B***, Stimulating electrode track with tip located in STN. ***C***, ***D***, Recording electrode tracks with tips located in SNr (***C***) and GPe (***D***). ***E***, Locations of stimulation electrode tips (red dots) used for bipolar stimulation ($n = 13$ rats). In all rats, at least one electrode used for bipolar stimulation was positioned within STN. STN, Dark gray; cerebral peduncle, light gray.

HFS produced both excitatory and inhibitory responses

There was no difference in the mean firing rate prelesion (healthy) compared with postlesion in either the GPe (Fig. 5*A*) or SNr (Fig. 5*B*). As well, there was no difference in the mean firing rate from DBS-off to DBS-on for any of the stimulation frequencies (Fig. 5*A*, *B*), nor did we observe any change in the number of recorded units between DBS-off and DBS-on. At the single-unit level, with responses normalized to their own baseline firing rate during the prestimulation and poststimulation periods, the number of single units that increased or decreased in firing rate during HFS increased with increasing frequency of DBS (Fig. 5*C*,*E*, GPe; Fig. 5*D*,*F*, SNr; Pearson's χ^2 test, $p < 0.05$). Thus, the dual effect of activation and inhibition during HFS resulted in a lack of significant change in the mean firing rate.

HFS disrupted low-frequency oscillations

Spectral analysis of single-unit firing times was used to quantify the effects of DBS frequency on oscillatory activity. Postlesion, in the absence of DBS, there was increased oscillatory activity centered at ~9 Hz (Fig. 6*A2*,*A3*, GPe; Fig. 6*D2*,*D3*, SNr). This oscillatory activity was not continuous in time and occurred in bouts during the prestimulation and poststimulation periods (Fig. 7*A*, GPe; Fig. 7*B*, SNr). The absence of any peak in this band during prelesion recordings suggests that the oscillations in postlesion recordings were indeed pathological (Fig. 6*A1*, GPe; Fig. 6*D1*, SNr). An analysis of the spectral power within a window encompassing this band showed that the peak was increased from prelesion to postlesion and was reduced only during HFS (Fig. 6*B*, GPe; Fig. 6*E*, SNr). During HFS, the oscillatory activity remained reduced for the entire duration of stimulation (Fig. 7*A5*,*A6*, GPe; Fig. 7*B5*,*B6*, SNr). However, within only seconds after HFS was turned off, the oscillations returned to prestimulation levels (Fig. 7*A5*,*A6*, GPe; Fig. 7*B5*,*B6*, SNr).

Eighteen of 62 (29.0%) GPe neurons showed increased low-frequency oscillations compared with the healthy population, and of these, 18 of 18 (100%) showed a decrease in low-frequency oscillations during 130 Hz DBS. Thirty-one of 51 (60.8%) SNr neurons showed increased low-frequency oscillations compared with the healthy population, and, of these, 22 of 31 (71.0%) showed a decrease in low-frequency oscillations during 130 Hz DBS.

HFS entrained neuronal firing patterns to the stimulation frequency

Spectral analysis of single-unit recordings was also used to quantify the effects of DBS frequency on oscillatory activity at the stimulation frequency. DBS resulted in a peak in spectral power at the stimulation frequency in GPe (Fig. 6*A2*,*A3*) and SNr (Fig. 6*D2*,*D3*), which was not present in prelesion (Fig. 6*A1*, GPe; Fig.

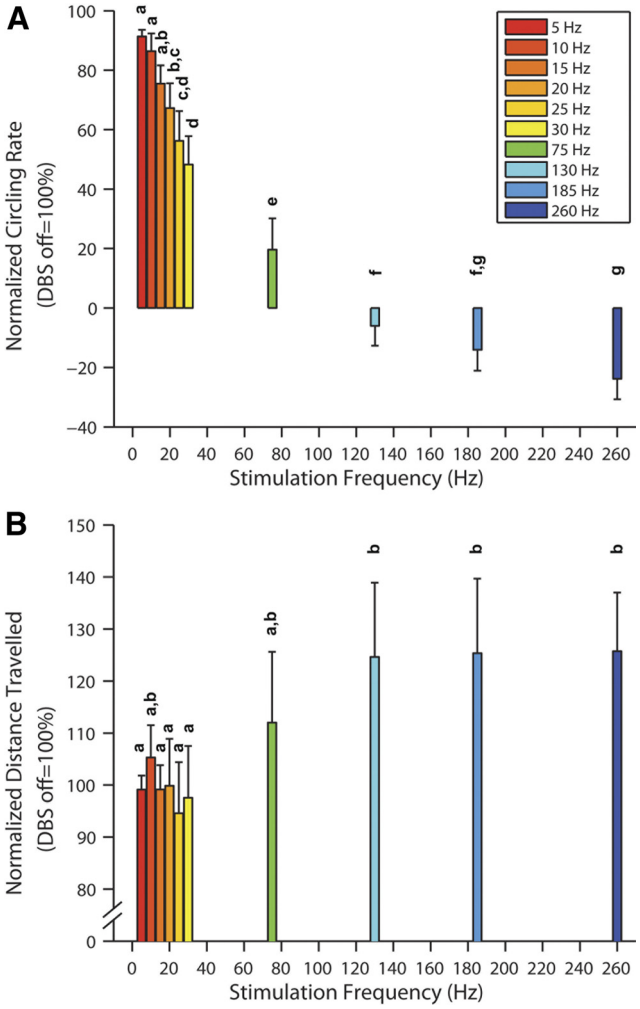

Figure 3. Effect of DBS frequency on methamphetamine-induced circling. ***A***, Effect of DBS frequency on circling rate across all rats (frequency was a significant factor $p < 0.05$, one-way repeated-measures ANOVA; different letters indicate significant differences $p < 0.05$, *post hoc* Fisher's PLSD). ***B***, Effect of DBS frequency on distance traveled across all rats (frequency was a significant factor $p < 0.05$, one-way repeated-measures ANOVA; different letters indicate significant differences $p < 0.05$, *post hoc* Fisher's PLSD). Bars represent mean ± SE ($n = 13$).

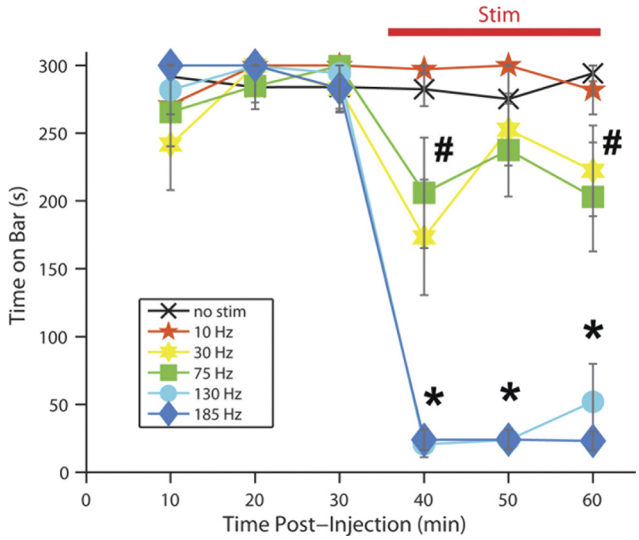

Figure 4. Effect of DBS frequency on haloperidol-induced akinesia. Asterisks indicate time points at which 130 and 185 Hz conditions were significantly different from all other conditions ($p < 0.05$, two-way repeated-measures ANOVA; $p < 0.05$, *post hoc* Fisher's PLSD). Hash marks indicate time points at which 30 and 75 Hz conditions were significantly different from all other conditions ($p < 0.05$, two-way repeated-measures ANOVA; $p < 0.05$, *post hoc* Fisher's PLSD). Bars represent mean ± SE ($n = 11$).

6*D1*, SNr) or postlesion recordings (Fig. 6*A2*,*A3*, GPe; Fig. 6*D2*,*D3*, SNr).

DBS significantly increased oscillation activity at 30, 75, 130, and 185 Hz compared with DBS-off (Fig. 6*C*, GPe; Fig. 6*F*, SNr). The magnitude of the peak increased with increasing frequency and was greatest for HFS (Fig. 6*C*, GPe; Fig. 6*F*, SNr). During 130 Hz effective STN-DBS, 37 of 62 (59.7%) GPe neurons and 39 of 51 (76.5%) SNr neurons showed increased oscillatory power at the stimulation frequency. Interestingly, 5 Hz stimulation did not result in an increase in power at the stimulation frequency, as observed with other stimulation frequencies, but rather caused an increase in power at ~0–3 Hz.

In addition, we quantified the degree of synchronization between neuronal activity and the stimulation pulses by calculating vector strength (Goldberg and Brown, 1969). Vector strength increased with increasing stimulation frequency (Fig. 8*A*, GPe; Fig. 8*B*, SNr), indicating that HFS entrained neuronal firing patterns in the GPe and SNr to follow the stimulation pulses more effectively than LFS.

Relationship between firing rate and oscillatory pattern

We investigated the relationship between changes in firing rate and changes in oscillatory activity during 130 Hz STN-DBS. All units within GPe or SNr were grouped into one of three categories based on their firing rate response during 130 Hz stimulation: excited, inhibited, or no change. The spectral power within each category was then integrated over 7–10 Hz and 129–131 Hz (stimulation frequency ± 1 Hz). No significant interaction between firing rate response and oscillatory power during DBS at 130 Hz was found for either of the frequency ranges (two-way repeated-measures ANOVA; GPe, 7–11 Hz: $p = 0.28$; SNr 7–11 Hz: $p = 0.07$; GPe 128–132 Hz: $p = 0.34$; SNr 128–132 Hz: $p = 0.99$).

HFS shifted the coherence from the low-frequency band to the stimulation frequency

We quantified the effects of stimulation frequency on coherence between simultaneously recorded pairs of neurons within and across the GPe and SNr in the 7–10 Hz band and in the band at the stimulation frequency. A larger proportion of neuron pairs decreased in coherence in the 7–10 Hz band during HFS compared with LFS in both the GPe (Fig. 9*A1*) and the SNr (Fig. 9*A2*), and even more so for pairs across GPe and SNr (Fig. 9*A3*), and only LFS resulted in neuron pairs with increased coherence in the 7–10 Hz band (Fig. 9*A1–A3*).

The predominant effect of HFS was increased coherence at the stimulation frequency both within and across the GPe and SNR (Fig. 9*B1–B3*), and few neuron pairs decreased coherence in the stimulation frequency band for any of the stimulation frequencies. HFS had a larger effect than LFS on increased coherence at the stimulation frequency within the GPe (Fig. 9*B1*), within the SNr (Fig. 9*B2*), and across the GPe and SNr (Fig. 9*B3*).

Discussion

The clinical effects of DBS are strongly dependent on stimulation frequency, but the neuronal basis of this dependence is unclear. We quantified the effects of STN-DBS frequency on motor behavior and single-unit activity in the GPe and SNr of hemiparkinsonian rats. Using two separate behavioral tasks, we observed frequency tuning curves similar to those observed clinically in humans with PD.

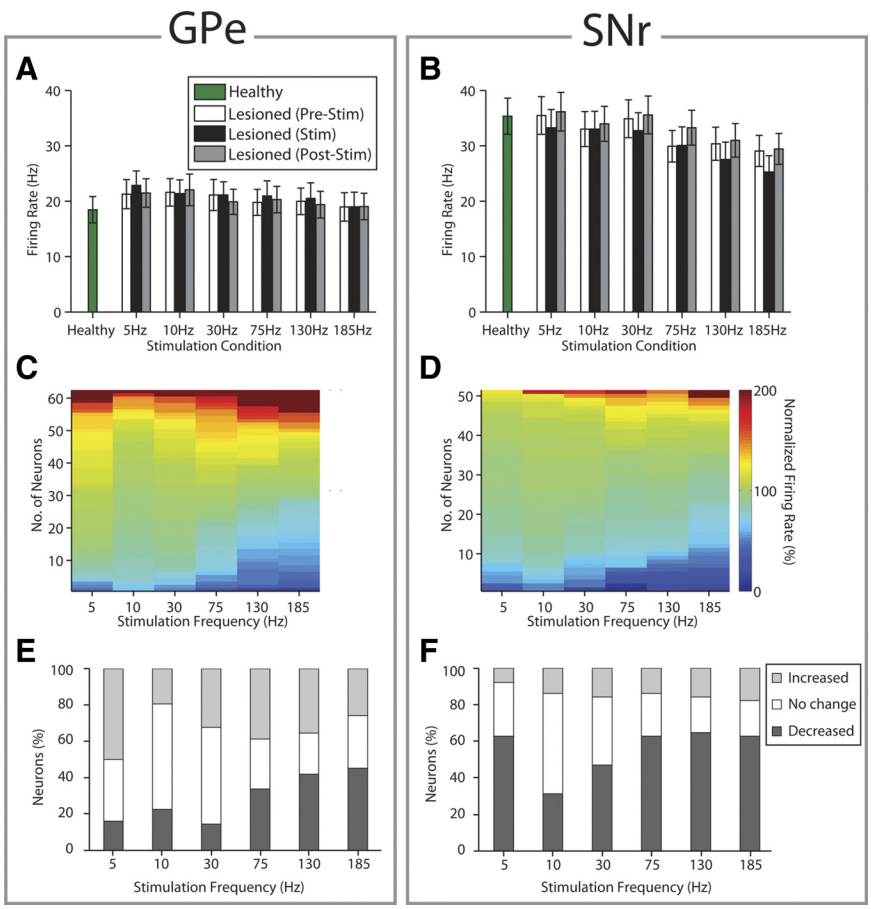

Figure 5. ***A–F***, Effects of DBS frequency on neuronal firing rates in GPe (***A***, ***C***, ***E***) and SNr (***B***, ***D***, ***F***). ***A***, ***B***, Mean firing rate for GPe (***A***) and SNr (***B***). No difference in mean firing rate was observed between healthy and lesion conditions in either region, or between DBS-off and DBS-on at any frequency in either region (two-way repeated-measures ANOVA). ***C***, ***D***, Firing rate for individual neurons (a single row in colorplot represents one neuron) normalized to DBS-off firing rate in GPe (***C***) and SNr (***D***). Color maps are sorted based on response during stimulation from most inhibitory to most excitatory within each stimulation condition. Note increase in number of neurons with either excitatory or inhibitory responses with increasing stimulation frequency. ***E***, ***F***, Categorization of individual neurons in GPe (***E***) and SNr (***F***) based on change in firing rates. Difference in percentage of neurons with decreased, increased, or no change in firing rates across various frequencies of stimulation was significant (Pearson's χ^2 test, $p < 0.05$). Bars represent mean ± SE (GPe: healthy, $n = 91$; postlesion, $n = 62$ and SNr: healthy, $n = 70$; postlesion, $n = 51$). Gray boxes separate results by the neural regions analyzed.

Single-unit recordings revealed that DBS had mixed effects on firing rate, with an increase in both excitatory and inhibitory responses as the frequency was increased. Thus, changes in firing rate did not explain the frequency-dependent behavioral effects of DBS. Rather, changes in patterns of neuronal activity were strongly dependent on DBS frequency and correlated strongly with behavioral efficacy. HFS, but not LFS, synchronized firing with the stimulus pulses and reduced pathological oscillations in the 7–10 Hz band. Our results support the hypothesis that effective STN-DBS suppresses pathological firing patterns and induces a new pattern of activity characterized by regularized firing at the stimulation frequency.

Effect of DBS frequency on behavior

The behavioral effects of STN-DBS were strongly dependent on the stimulation frequency. Unilateral 6-OHDA lesioning induced pathological turning ipsilateral to the lesion (Richards et al., 1990), which was exacerbated by methamphetamine. Applying high-frequency DBS effectively reversed circling bias without decreasing overall movement. These results corroborate other reports of reduced ipsilateral and/or increased contralateral circling in response to STN-HFS (Meissner et al., 2002; Gradinaru et al., 2009). Similarly, akinesia induced by the dopamine antagonist haloperidol was effectively reversed by HFS. Importantly, we observed that LFS was not as effective as HFS in alleviating either methamphetamine-induced circling or haloperidol-induced akinesia, and this frequency dependence of symptom alleviation was consistent with clinical observations in persons with PD (Moro et al., 2002; Timmermann et al., 2004; Fogelson et al., 2005; Eusebio et al., 2008).

Effect of DBS frequency on firing rates of basal ganglia neurons

HFS elicited both increases and decreases in the firing rate of neurons in the GPe and SNr. Due to these opposing effects on firing rate, there was no net change in the mean firing rates of the GPe and SNr during DBS at any frequency, including behaviorally effective HFS. Previous studies reported contradictory results regarding the effects of DBS on neuronal firing rates. In MPTP-treated monkeys, an increase in GP interna (GPi) activity was reported (Hashimoto et al., 2003), although effects were variable across neurons (Dorval et al., 2008), while in normal (Burbaud et al., 1994; Benazzouz et al., 1995) and 6-OHDA-lesioned rats (Benazzouz et al., 2000) nearly complete inhibition in the SNr was reported during HFS. Other groups have reported no net change in firing rate during HFS in the GPe, GPi/SNr (Bosch et al., 2011), or both (Shi et al., 2006; Moran et al., 2011). Our results across a large number of single units support the hypothesis that STN-DBS results in both activation and inhibition of neurons within the GPe and SNr. Although effective high-frequency DBS resulted in a greater proportion of neurons with changes in firing rates compared with low-frequency DBS, changes in the mean firing rate did not explain the frequency dependence of the behavioral effects of DBS.

The dual effect of STN-DBS likely resulted from coactivation of different neuron populations. GABAergic fibers projecting from GPe to SNr pass through the STN (Bosch et al., 2011), and activation of passing pallidonigral fibers may have contributed to inhibition in the SNr, while excitation was likely due to activation of glutamatergic projections from the STN to SNr. Further support for this explanation comes from studies on changes in neurotransmitter concentration during DBS. Extracellular concentrations of both glutamate and GABA in the SNr and GPe increased during STN-HFS (Windels et al., 2000, 2003), and lesioning the GPe abolished the increase in GABA in the SNr (Windels et al., 2005), supporting the role of GPe–SNr connections in STN-DBS-mediated inhibition of the SNr.

Effect of DBS frequency on suppression of low-frequency oscillations

The 7–10 Hz oscillations observed following 6-OHDA lesioning were not present in the healthy condition, which implies that these oscillations were pathological. Furthermore, low-frequency oscilla-

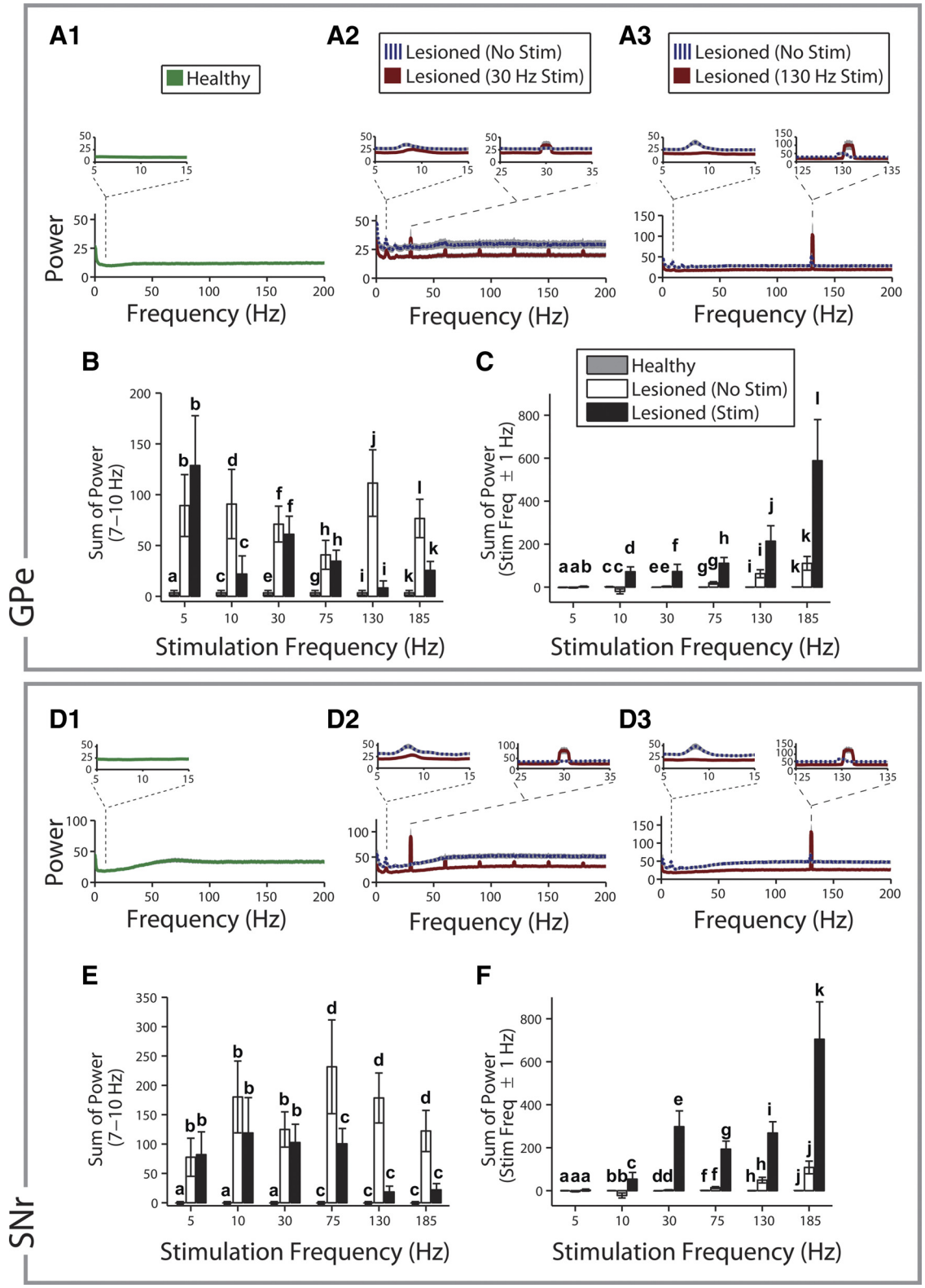

Figure 6. ***A–F***, Effects of DBS frequency on neuronal oscillations quantified from power spectra of single-unit firing times in GPe (***A–C***) and SNr (***D–F***). ***A***, ***D***, Power spectra for healthy (***A1***, ***D1***) and lesioned rats with and without stimulation at 30 Hz (***A2***, ***D2***) and 130 Hz (***A3***, ***D3***). Insets are zoomed views (5–15, 25–35, or 125–135 Hz) of wider frequency range (0 –200 Hz). Peak centered at ~9 Hz was present in both GPe (***A2***, ***A3***) and SNr (***D2***, ***D3***) in lesioned rats with no stimulation. Peak was not present in healthy condition (***A1***, ***D1***), and HFS reduced these low-frequency oscillations in GPe (***A3***) and SNr (***D3***). Peaks in spectrum at the stimulation frequency increased in magnitude during DBS in both GPe (***A2***, ***A3***) and SNr (***D2***, ***D3***). Lines represent mean (colored) ± SE (shaded gray) (GPe: healthy, $n = 91$; postlesion, $n = 62$ and SNr: healthy, $n = 70$; postlesion, $n = 51$). ***B***, ***C***, ***E***, ***F***, Sum of spectral power over low-frequency (7–10 Hz) (***B***, ***E***) and stimulation frequency (stimulation frequency ± 1 Hz) (***C***, ***F***) bands in GPe (***B***, ***C***) and SNr (***E***, ***F***). HFS reduced low-frequency oscillations (***B***, ***E***) and increased oscillatory activity at stimulation frequency (***C***, ***F***) ($p < 0.05$, two-way repeated-measures ANOVA; Different letters indicate significant differences $p < 0.05$, *post hoc* Fisher's PLSD). Bars represent mean ± SE (GPe: healthy, $n = 91$; postlesion, $n = 62$ and SNr: healthy, $n = 70$; postlesion, $n = 51$). ***D***, ***E***, and ***F*** use the same figure legends as ***A–C***. Gray boxes separate results by the neural regions analyzed.

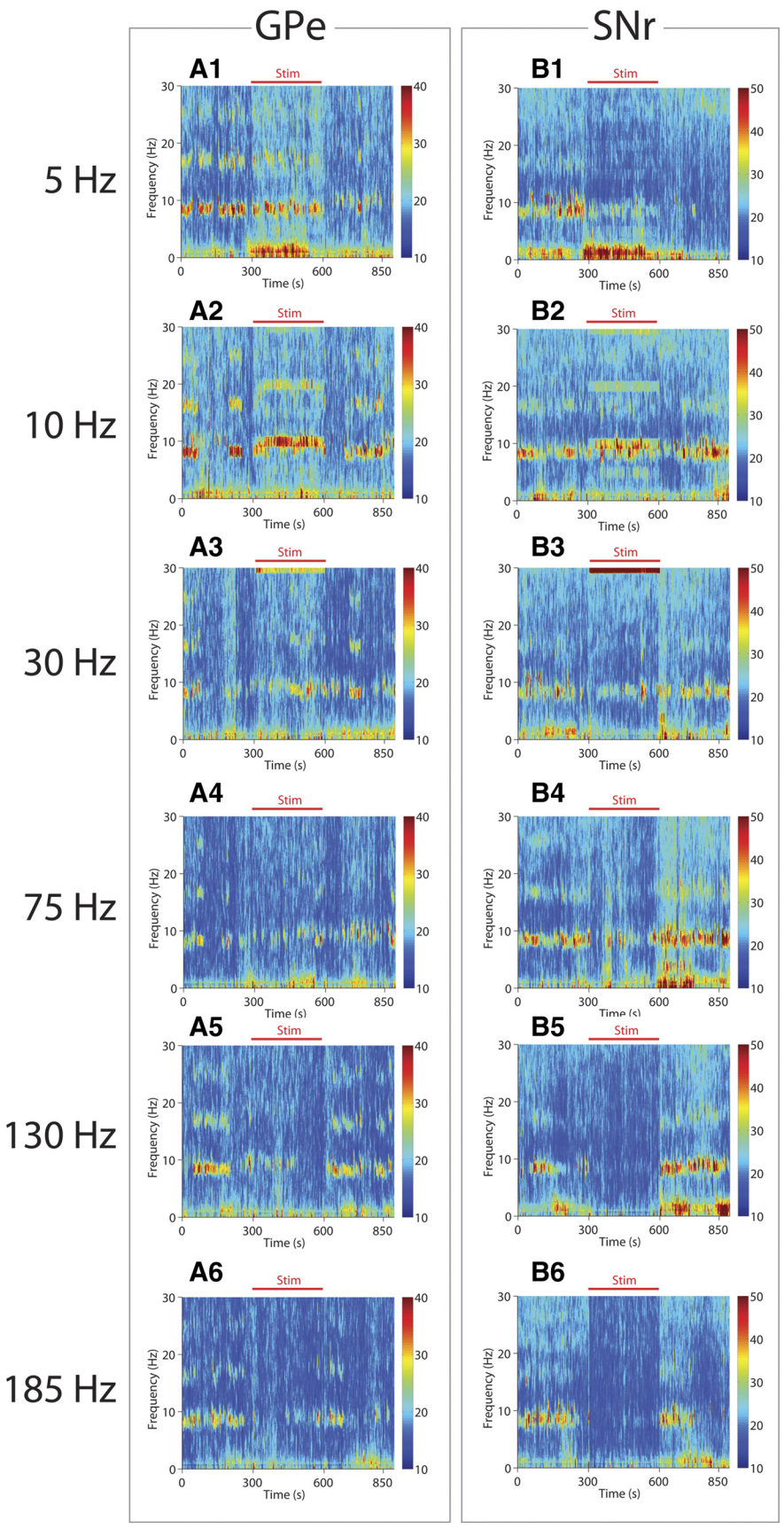

Figure 7. ***A1–B6***, Time-frequency spectrograms showing effect of DBS on low-frequency neuronal oscillations in GPe (***A1–A6***) and SNr (***B1–B6***). Plots show mean spectral power (GPe = 62 neurons; SNr = 51 neurons). Color bar indicates spectral power. Note inhibition of low-frequency oscillations (7–10 Hz) during HFS (***A5***, ***A6***, GPe; ***B5***, ***B6***, SNr). Gray boxes separate results by the neural regions analyzed.

tions were reduced during behaviorally effective HFS, but not during ineffective LFS. This oscillatory activity may be associated with resting tremor, since 8–10 Hz head and neck tremor at rest was correlated with rhythmic 8–10 Hz oscillations in cortex in 6-OHDA-lesioned rats (Buonamici et al., 1986). As well, a recent study in MPTP monkeys reported a correlation between suppression of low-frequency oscillations [in the theta (4–7 Hz) and alpha (9–15 Hz) bands] and improvements in motor symptoms during 130 Hz DBS (Rosin et al., 2011).

Although neuronal recordings were performed when rats were at rest and not during behavioral tasks, this enabled us to record the activity of neurons without the influence of any drugs (i.e., methamphetamine, haloperidol). The recordings were performed during DBS at amplitudes that elicited meaningful behavioral responses, and recordings were obtained from the same set of neurons under various stimulation conditions in each rat. We previously studied the effect of stimulation amplitude at 130 Hz on circling (So et al., 2012a). To understand further the effects of stimulation amplitude on neural activity, we analyzed the effect of stimulation amplitude on low-frequency oscillations (7–10 Hz) in a subset of 25 units recorded from the SNr in four rats across five different amplitudes. Results from five different amplitudes at 130 Hz (50%, 80%, 100%, 110%, and 130% of the minimum stimulation amplitude threshold to elicit a behavioral response) showed that, relative to the 50% amplitude, the mean low-frequency oscillatory power was increased by 6% (±48% SEM) during 80% stimulation amplitude, while the power was reduced by 85% (±13% SEM), 107% (±8% SEM), and 108% (±4% SEM) during 100%, 110%, and 130% stimulation amplitudes, respectively. These results, together with our behavioral observations of the effects of DBS amplitude on circling (So et al., 2012a), validate our selection criteria for stimulation amplitude and suggest that DBS was more effective at reducing low-frequency power at stimulation amplitudes above 100% stimulation threshold compared with lower amplitudes.

Effect of DBS frequency on entrainment of basal ganglia neurons

Spectral analysis revealed that DBS resulted in increased neuronal oscillations at the stimulation frequency in the GPe and SNr. These increased oscillations were more pronounced during HFS than during LFS. Furthermore, calculations of vector strength showed that HFS resulted

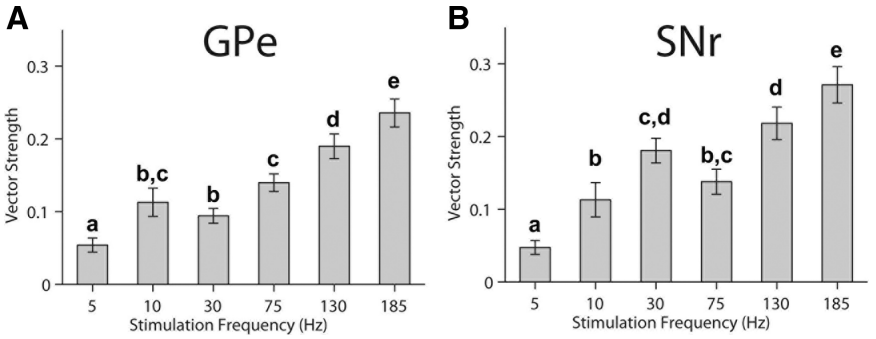

Figure 8. Effect of DBS frequency on phase locking of neuronal firing to the stimulus pulse as measured by vector strength. HFS was associated with high vector strength, indicating that neuronal activity was more synchronized with stimulation pulses during HFS. Bars represent mean ± SE ($p < 0.05$, one-way repeated-measures ANOVA. Different letters indicate significant differences $p < 0.05$, *post hoc* Fisher's PLSD. GPe = 62 neurons; SNr = 51 neurons).

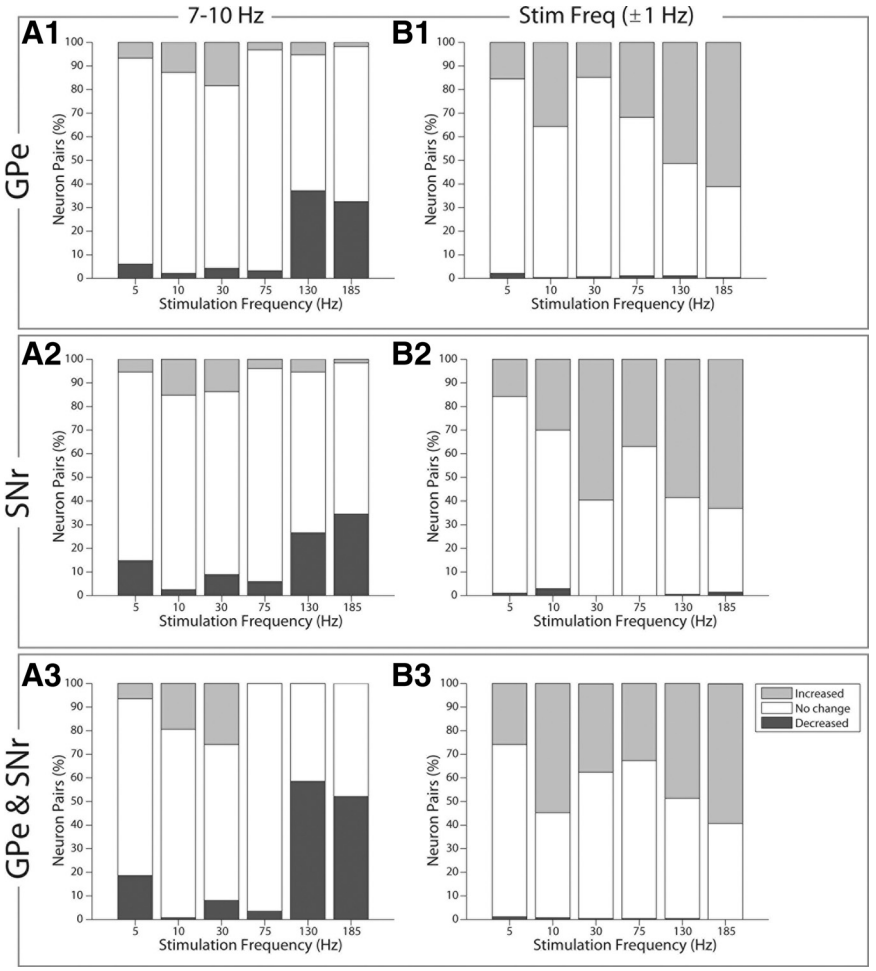

Figure 9. Effect of DBS frequency on coherence between pairs of simultaneously recorded neurons within and across GPe and SNr. ***A1–B3***, The percentage of neuron pairs categorized as showing decreased, no change, or increased coherence during DBS with different stimulation frequencies within GPe (***A1***, ***B1***), SNr (***A2***, ***B2***), and across GPe and SNr (***A3***, ***B3***). Within GPe (***A1***) and within SNr (***A2***), DBS at stimulation frequencies ≤75 Hz decreased coherence in the 7–10 Hz band less than stimulation frequencies ≥130 Hz. Within GPe (***B1***) and within SNr (***B2***), there was a trend toward increased coherence in the stimulation band with increased stimulation frequency. ***A3***, Across GPe and SNr, DBS at stimulation frequencies ≤75 Hz decreased coherence in the 7–10 Hz band less than stimulation frequencies ≥130 Hz. ***B3***, Across GPe and SNr, there was a trend toward increased coherence in the stimulation band with increased stimulation frequency. Difference in percentage of neurons with decrease, increase, or no change in coherence across frequencies of stimulation was significant (Pearson's χ^2 test, $p < 0.05$; GPe: 283 unique neuronal pairs across 7 rats; SNr: 203 unique neuronal pairs across 6 rats; GPe and SNr: 263 unique neuronal pairs across 3 rats). Gray boxes separate results by the neural regions analyzed.

in greater phase locking between neuronal spikes and stimulus pulses compared with LFS. These results indicate that neurons were synchronized to the stimulus pulses, and this entrainment was more pronounced during high-frequency DBS.

Previous studies also reported neuronal firing time locked to the stimulus pulses during HFS. Stimulation of the STN in brain slices caused STN neurons to fire synchronously with the stimulation pulses (Garcia et al., 2005). In MPTP-treated monkeys, STN-DBS generated stereotyped discharge patterns within the GPe and GPi, with peaks at integer multiples of the interpulse interval in the ISI histograms (Hashimoto et al., 2003). Similarly, STN-DBS in a patient with PD resulted in GPi neuronal responses that were time locked to the stimulation pulses (Reese et al., 2011).

Effect of DBS frequency on coherence of oscillatory activity

The shift in neuronal oscillatory activity from the pathological 7–10 Hz band to the stimulation frequency during behaviorally effective HFS was observed in single neurons and at the network level. Synchronization of oscillatory activity in the basal ganglia is a hallmark of PD (Levy et al., 2000, 2002a,b; Brown et al., 2001). Our results indicate that during HFS these pathological oscillations are weakened, or decoupled, between structures of the basal ganglia and strengthened, or coupled, at the stimulation frequency. In support of this hypothesis, STN-HFS in primates reduces coherence between the STN and GPi (Moran et al., 2012). Though Moran et al. (2012) suggested that the decoupling action of STN-HFS would cause GPi to resume an independent neuronal activity pattern, our results indicate that the activity was not independent, but rather driven by the stimulation frequency.

In summary, we observed a correlation between the stimulation frequency-dependent behavioral effects of DBS and the stimulation frequency-dependent effects on suppression of low-frequency oscillations, neural entrainment to the stimulation pulses, and reduced low-frequency coherence across the basal ganglia. The changes in firing patterns in the GPe and SNr during DBS were independent of changes in firing rates. These results support the hypothesis that the mechanism for the effectiveness of DBS lies in its ability to entrain neurons to fire in a regularized manner, hence suppressing intrinsic pathological patterns of activity and creating an "informational lesion" (Grill et al., 2004). While the resulting firing patterns within the basal ganglia do not resemble firing patterns in healthy subjects, they are less pathological than those in PD.

References

Benazzouz A, Piallat B, Pollak P, Benabid AL (1995) Responses of substantia nigra pars reticulata and globus pallidus complex to high frequency stimulation of the subthalamic nucleus in rats: electrophysiological data. Neurosci Lett 189:77–80.

Benazzouz A, Gao DM, Ni ZG, Piallat B, Bouali-Benazzouz R, Benabid AL (2000) Effect of high-frequency stimulation of the subthalamic nucleus on the neuronal activities of the substantia nigra pars reticulata and ventrolateral nucleus of the thalamus in the rat. Neuroscience 99:289–295.

Birdno MJ, Grill WM (2008) Mechanisms of deep brain stimulation in movement disorders as revealed by changes in stimulus frequency. Neurotherapeutics 5:14–25.

Bokil H, Purpura K, Schoffelen J-M, Thomson D, Mitra P (2007) Comparing spectra and coherences for groups of unequal size. J Neurosci Methods 159: 337–345.

Bosch C, Degos B, Deniau JM, Venance L (2011) Subthalamic nucleus high frequency stimulation generates a concomitant synaptic excitation-inhibition in substantia nigra pars reticulata. J Physiol 589:4189–4207.

Breese GR, Traylor TD (1971) Depletion of brain noradrenaline and dopamine by 6-hydroxydopamine. Br J Pharmacol 42:88–99.

Brown P, Oliviero A, Mazzone P, Insola A, Tonali P, Di Lazzaro V (2001) Dopamine dependency of oscillations between subthalamic nucleus and pallidum in Parkinson's disease. J Neurosci 21:1033–1038.

Buonamici M, Maj R, Pagani F, Rossi AC, Khazan N (1986) Tremor at rest episodes in unilaterally 6-OHDA-induced substantia nigra lesioned rats: EEG-EMG and behavior. Neuropharmacology 25:323–325.

Burbaud P, Gross C, Bioulac B (1994) Effect of subthalamic high frequency stimulation on substantia nigra pars reticulata and globus pallidus neurons in normal rats. J Physiol Paris 88:359–361.

Deuschl G, Schade-Brittinger C, Krack P, Volkmann J, Schäfer H, Bötzel K, Daniels C, Deutschländer A, Dillmann U, Eisner W, Gruber D, Hamel W, Herzog J, Hilker R, Klebe S, Kloss M, Koy J, Krause M, Kupsch A, Lorenz D, et al. (2006) A randomized trial of deep-brain stimulation for Parkinson's disease. N Engl J Med 355:896–908.

Dorval AD, Russo GS, Hashimoto T, Xu W, Grill WM, Vitek JL (2008) Deep brain stimulation reduces neuronal entropy in the MPTP-primate model of Parkinson's disease. J Neurophysiol 100:2807–2818.

Eusebio A, Chen CC, Lu CS, Lee ST, Tsai CH, Limousin P, Hariz M, Brown P (2008) Effects of low-frequency stimulation of the subthalamic nucleus on movement in Parkinson's disease. Exp Neurol 209:125–130.

Fogelson N, Kühn AA, Silberstein P, Limousin PD, Hariz M, Trottenberg T, Kupsch A, Brown P (2005) Frequency dependent effects of subthalamic nucleus stimulation in Parkinson's disease. Neurosci Lett 382:5–9.

Garcia L, D'Alessandro G, Fernagut PO, Bioulac B, Hammond C (2005) Impact of high-frequency stimulation parameters on the pattern of discharge of subthalamic neurons. J Neurophysiol 94:3662–3669.

Goldberg JM, Brown PB (1969) Responses of binaural neurons of dog superior olivary complex to dichotic tonal stimulation: some physiological mechanisms of sound localization. J Neurophysiol 32:940–958.

Gradinaru V, Mogri M, Thompson KR, Henderson MJ, Deisseroth K (2009) Optical deconstruction of parkinsonian neural circuitry. Science 324: 354–359.

Grill WM, Snyder AN, Miocinovic S (2004) Deep brain stimulation creates an informational lesion of the stimulated nucleus. Neuroreport 15:1137–1140.

Hashimoto T, Elder CM, Okun MS, Patrick SK, Vitek JL (2003) Stimulation of the subthalamic nucleus changes the firing pattern of pallidal neurons. J Neurosci 23:1916–1923.

Levy R, Hutchison WD, Lozano AM, Dostrovsky JO (2000) High-frequency synchronization of neuronal activity in the subthalamic nucleus of parkinsonian patients with limb tremor. J Neurosci 20:7766–7775.

Levy R, Hutchison WD, Lozano AM, Dostrovsky JO (2002a) Synchronized neuronal discharge in the basal ganglia of parkinsonian patients is limited to oscillatory activity. J Neurosci 22:2855–2861.

Levy R, Ashby P, Hutchison WD, Lang AE, Lozano AM, Dostrovsky JO (2002b) Dependence of subthalamic nucleus oscillations on movement and dopamine in Parkinson's disease. Brain 125:1196–1209.

McIntyre CC, Hahn PJ (2010) Network perspectives on the mechanisms of deep brain stimulation. Neurobiol Dis 38:329–337.

Meissner W, Harnack D, Paul G, Reum T, Sohr R, Morgenstern R, Kupsch A (2002) Deep brain stimulation of subthalamic neurons increases striatal dopamine metabolism and induces contralateral circling in freely moving 6-hydroxydopamine-lesioned rats. Neurosci Lett 328:105–108.

Mitra PP, Pesaran B (1999) Analysis of dynamic brain imaging data. Biophysical journal 76:691–708.

Moran A, Stein E, Tischler H, Belelovsky K, Bar-Gad I (2011) Dynamic stereotypic responses of basal ganglia neurons to subthalamic nucleus high-frequency stimulation in the parkinsonian primate. Front Syst Neurosci 5:21.

Moran A, Stein E, Tischler H, Bar-Gad I (2012) Decoupling neuronal oscillations during subthalamic nucleus stimulation in the parkinsonian primate. Neurobiol Dis 45:583–590.

Moro E, Esselink RJ, Xie J, Hommel M, Benabid AL, Pollak P (2002) The impact on Parkinson's disease of electrical parameter settings in STN stimulation. Neurology 59:706–713.

Paxinos G, Watson C (2007) The rat brain in stereotaxic coordinates, Ed 6. San Diego: Academic.

Reese R, Leblois A, Steigerwald F, Pötter-Nerger M, Herzog J, Mehdorn HM, Deuschl G, Meissner WG, Volkmann J (2011) Subthalamic deep brain stimulation increases pallidal firing rate and regularity. Experimental neurology 229:517–521.

Richards JB, Sabol KE, Freed CR (1990) Unilateral dopamine depletion

causes bilateral deficits in conditioned rotation in rats. Pharmacol Biochem Behav 36:217–223.

Rosin B, Slovik M, Mitelman R, Rivlin-Etzion M, Haber SN, Israel Z, Vaadia E, Bergman H (2011) Closed-loop deep brain stimulation is superior in ameliorating parkinsonism. Neuron 72:370–384.

Rubin JE, Terman D (2004) High frequency stimulation of the subthalamic nucleus eliminates pathological thalamic rhythmicity in a computational model. J Comput Neurosci 16:211–235.

Sanberg PR, Bunsey MD, Giordano M, Norman AB (1988) The catalepsy test: its ups and downs. Behav Neurosci 102:748–759.

Schwarting RK, Huston JP (1996) The unilateral 6-hydroxydopamine lesion model in behavioral brain research. Analysis of functional deficits, recovery and treatments. Prog Neurobiol 50:275–331.

Shi LH, Luo F, Woodward DJ, Chang JY (2006) Basal ganglia neural responses during behaviorally effective deep brain stimulation of the subthalamic nucleus in rats performing a treadmill locomotion test. Synapse 59:445–457.

So RQ, McConnell GC, August AT, Grill WM (2012a) Characterizing effects of subthalamic nucleus deep brain stimulation on methamphetamine-induced circling behavior in hemiparkinsonian rats. IEEE Trans Neural Syst Rehabil Eng 20:626–635.

So RQ, Kent AR, Grill WM (2012b) Relative contributions of local cell and passing fiber activation and silencing to changes in thalamic fidelity during deep brain stimulation and lesioning: a computational modeling study. J Comput Neurosci 32:499–519.

Terman D, Rubin JE, Yew AC, Wilson CJ (2002) Activity patterns in a model for the subthalamopallidal network of the basal ganglia. J Neurosci 22:2963–2976.

Timmermann L, Wojtecki L, Gross J, Lehrke R, Voges J, Maarouf M, Treuer H, Sturm V, Schnitzler A (2004) Ten-hertz stimulation of subthalamic nucleus deteriorates motor symptoms in Parkinson's disease. Mov Disord 19:1328–1333.

Windels F, Bruet N, Poupard A, Urbain N, Chouvet G, Feuerstein C, Savasta M (2000) Effects of high frequency stimulation of subthalamic nucleus on extracellular glutamate and GABA in substantia nigra and globus pallidus in the normal rat. Eur J Neurosci 12:4141–4146.

Windels F, Bruet N, Poupard A, Feuerstein C, Bertrand A, Savasta M (2003) Influence of the frequency parameter on extracellular glutamate and gamma-aminobutyric acid in substantia nigra and globus pallidus during electrical stimulation of subthalamic nucleus in rats. J Neurosci Res 72:259–267.

Windels F, Carcenac C, Poupard A, Savasta M (2005) Pallidal origin of GABA release within the substantia nigra pars reticulata during high-frequency stimulation of the subthalamic nucleus. J Neurosci 25:5079–5086.